AUTOMATED SCREENING OF CHEST X RAYS: TEXTURE ANALYSIS OF THE LUNG FIELDS IN CHEST X RAYS*

T. W. Challis
Department of Diagnostic Radiology

C. M. Haig
D. C. Haig
J. H. Kulick
Department of Computing and Information Science
Queen's University
Kingston, Ontario
Canada K7L 3N6

Abstract

This paper describes one part of a system for automatically analysing chest x-rays. Previous publications have described the hardware, rib border detection and preliminary results for analysis of the lung fields. This paper is concerned with texture analysis and classification of the lung fields of chest x-rays. A description of the algorithms and some preliminary results are presented.

Introduction

The goal of the system being developed at Queen's University is to classify films as normal or abnormal, returning abnormal films to a radiologist for examination. The analysis of the lung fields is, of course, a major aspect in such a system. Previous studies concerned with the lungs in x-rays have been of two distinct types: those that locate structures in the lungs and those that examine the texture of the lungs. Structures that have been the focus of studies include: circular tumours, small rounded opacities (10) and blood vessels in the hilar regions (3). Texture measures have been used to classify various pathologies of the lungs including: pneumoconiosis (5,6,7,9,11); pulmonary edema (1); venus hypertension (4); interstitial fibrosis (12); and pulmonary infiltration.

In a screening environment, all types of diseases can be expected. It is therefore necessary to develop algorithms that are independent of a particular disease category. It would be valuable to know if a particular set of texture measures and a given method of study were able to distinguish normals from abnormals for many categories of lung disease and also to determine which types of abnormalities were not detectable using these texture measures and the given method of study. By isolating those abnormalities it might then be possible to develop further techniques to facilitate the detection of all diseases. This study is a preliminary one in which a group of texture measures is used to classify a set of x-rays that contains several disease categories.

Method of Study

Our approach is to identify the areas utilized by radiologists such as intercostal spaces, and to process them by using relationships similar to those used by radiologists. In particular we are examining the intercostal spaces in small disjoint regions (or zones) of the lung and are comparing individual regions between films, bilaterally opposite pairs of zones within a film and also horizontally and vertically adjacent pairs of zones within the same lung. While the classification of both individual zones and pairs of zones has been studied with some success by a number of investigators (4,5,7,1,12), these investigators do not use anatomically significant zones from both lung fields. The regions for this study are formed by separating the lungs into twelve zones as shown in Figure 1. Each zone contains only intercostal tissue and regions where ventral rib and lung overlap are treated as lung. The inner zones contain hilar blood vessesl which are large; the middle zones contain the medium sized blood vessels; and the outer zones contain small blood vessels which are barely detectable on the usual x-ray. The division into upper and lower zones occurs at the dorsal rib that is closest to the hila. The hila is chosen to be midway between the apices and the diaphragm. The inner, middle and outer zones are formed by 'shrinking' the lung boundaries. That is, if a line is drawn from the hila to a point on the lung border then the distance from the hila to the border between

* This project has been funded in part by Queen's University Advisory Research Committee, by Medical Research Council of Canada grant MA5614 and by National Research Council of Canada grant A9279.

Downloaded From: http://proceedings.spiedigitallibrary.org/ on 06/16/2016 Terms of Use: http://spiedigitallibrary.org/ss/TermsOfUse.aspx

the inner and middle zones is one-third of the distance from the hila to the lung border and the distance from the hila to the border between the middle and outer zones is two-thirds of the distance to the lung border. The rib borders are represented using quadratic polynomials that are reconstructed from three points on each border. For this study the three points for each rib border were located interactively. The lung, heart and diaphragm borders were located automatically by the segmentation module of the system.

Texture Measures

Two kinds of texture measures have been used by other investigators: those computed in the Fourier domain and those computed in the spatial or image domain domain. For a detailed discussion of texture measures, we refer the reader to Weska(14). There are several anomalies associated with Fourier measures, which include problems of false edges due to non-periodic data and the need for regular (rectangular or circular) regions of data points for comparison. Because of these anomalies, we have directed our attention primarily to measures that can be computed in the spatial domain. This technique allows for the rejection of individual pixels if, for example, a rib just grazes a sample area. This is not possible with the Fourier techniques.

The texture measures used in this study are the first order mean and variance of the gray levels and a variety of measures based on gray level difference statistics (14). The first order mean and variance are defined as:

$$\text{Mean} = \sum_{i=1}^{N_g} i\,g(i) \tag{1}$$

$$\text{Var} = \sum_{i=1}^{N_g} i^2 g(i) - \text{Mean}^2 \tag{2}$$

where $g(i)$ is the estimated probability distribution of the gray values of the image and N_g is the number of gray levels.

The difference statistics are defined as follows. Let $f(x,y)$ denote the image which has been digitized to N_g gray levels. Let $w = (\Delta x,\Delta y)$ be a vector in the (x,y) plane; the values of x and y are restricted to integers. For a given w the difference image $f_w(x,y)$ is calculated as:

$$f_w(x,y) = |f(x,y) - f(x+\Delta x, y+\Delta y)| \tag{3}$$

The difference image obtained will depend on both the size and the angle of the vector w. Possible types of difference images are listed below.

w	$f_w(x,y)$
(n,0)	horizontal (0^0) difference image
(n,n)	right diagonal (45^0) difference image
(0,n)	vertical (90^0) difference image
(n,-n)	left diagonal (135^0) difference image

The distance between points used to calculate the horizontal and vertical difference images is n. For the diagonal images this distance is $\sqrt{n}$. These difference images and the texture measures based on them are not sensitive to rotations of 180^0.

Let P_w be the probability density of $f_w(x,y)$. This takes the form of a one-dimensional array with N_g elements. The i-th element of P_w gives the probability that $f_w(x,y)=i$. In terms of the original image $f(x,y)$, $P_w(i)$ gives the probability that the gray levels of a pair of points which are w apart differ by i.

Downloaded From: http://proceedings.spiedigitallibrary.org/ on 06/16/2016 Terms of Use: http://spiedigitallibrary.org/ss/TermsOfUse.aspx

If the size of w is small relative to the size of texture elements in the image, then pairs of gray levels which are w apart should usually be similar and the values of P_w should be largest near i=0. If w is comparable to the size of texture elements, the values of P_w should be more spread out. If the texture is directional the distribution of values in P_w should vary for choices of w in different directions. Therefore measures which reflect the spread of values away from i=0 in P_w should give an indication of the coarseness of the texture in f(x,y) relative to the size of w. By varying the direction of w the directionality of the texture can be analyzed using these same measures.

The following difference measures are used.

1. $$\text{Dmean} = \sum_{i=0}^{N_g-1} iP_w(i)$$

This is the first moment of P_w about its origin. It is similar to the 'Mean' measure used by Weska [14] and the 'Edge' measure used by Chien [4] and Sutton [12].

2. $$\text{Contrast (Con)} = \sum_{i=0}^{N_g-1} i^2P_w(i)$$

This is the second moment of P_w about its origin. It is a measure of the spread of values away from i=0 in P_w [14].

3. $$\text{Angular Second Moment (Asm)} = \sum_{i=0}^{N_g-1} (P_w(i))^2$$

This measure will be smallest when the values of P_w are equal and larger if they differ [14].

4. $$\text{Entropy (Ent)} = -\sum_{i=0}^{N_g-1} P_w(i)\log(P_w(i))$$

This measure will be largest when the values of P_w are all equal and smaller when they are not [14].

The difference measures are calculated for eight choices of w (distance 1 and distance 2 for the four directions). Since the visible texture of the lungs is caused mainly by the blood vessels which fan out from the hila, the predominant direction of the texture in the upper zones is 90^0 different from that in the lower zones, and the texture in the right lung is 90^0 different from that in the left lung. To eliminate any problems this could cause, the four directions for w shall be considered to be: horizontal (0^0), vertical (90^0), parallel to the predominant direction of the texture (45^0 or 135^0, denoted by //) and perpendicular to the predominant direction of the texture (45^0 or 135^0, denoted by $\perp$). The thirty-four texture measures are calculated for each of the twelve zones shown in Figure 1.

Feature Extraction

The twelve zones of the lung fields are examined both individually and in pairs. The features used for the individual classification of the zones are chosen from the 34 texture measures. The features used for the pair-wise classification are chosen from ratios of these texture measures. The following types of ratios are considered.

1. Bilateral Inter-Lung

$$\frac{\text{Measure}_i(\text{zone}_{Lj})}{\text{Measure}_i(\text{zone}_{Rj})} \qquad \begin{matrix} i=1,\ldots.34 \\ j=1,\ldots.6 \end{matrix}$$

Downloaded From: http://proceedings.spiedigitallibrary.org/ on 06/16/2016 Terms of Use: http://spiedigitallibrary.org/ss/TermsOfUse.aspx

These ratios should give an indication of the bilateral asymmetry of the right and left lung fields. (If this ratio is greater than one, it is inverted. This removes differences caused by disease processes appearing in only the right or left lung.)

2. Horizontal Intra-Lung

$$\frac{\text{Measure}_i(\text{zone}_{Lj})}{\text{Measure}_i(\text{zone}_{Lk})} \qquad \begin{array}{l} i=1,\ldots.34 \\ j=1,2,4,5;\ k=j+1 \end{array}$$

Similar ratios are used for the right lung. These ratios should reflect the change in coarseness as you move from hilar to peripheral regions in either the left or the right lung.

3. Vertical Intra-Lung

$$\frac{\text{Measure}_i(\text{zone}_{Lj})}{\text{Measure}_i(\text{zone}_{Lk})} \qquad \begin{array}{l} i=1,\ldots.34 \\ j=1,2,3;\ k=j+3 \end{array}$$

Similar ratios are used for the right lung. These ratios should reflect the change in coarseness as you move from the upper to the lower zones of the lung fields. In a normal lung, the vessels in the lower regions are larger than those in the upper regions.

Data Set Description

The data available to test the classifiers consisted of fifty-one x-rays: twenty-three abnormal and twenty-eight normal. The abnormal films included samples from various pathologies. By including more than one disease category it is possible to evaluate the performance of the classifiers in a general screening environment. All films were of adult patients, including both males and females. The x-rays were diagnosed by a radiologist to obtain a classification for the films as well as for each of the zones. A pair of zones is considered abnormal if one or both of the zones is abnormal. For each classifier, all of the available abnormal samples and an equal number of normal samples were used.

The films used in this study were scanned into 512 x 512 arrays. This represents a scanning resolution of 1.5 lines/mm of film where each film is a standard 35 x 45 mm x-ray. Two hundred and fifty-six levels were used to quantize the gray levels of the image. To remove differences in the x-rays caused by variations in lightness, exposure time or digitization technique, the portion of the x-ray inside the lung boundaries was normalized to 64 equally probably gray levels.

Classification Results

Since the number of abnormal samples in some of the sets of data is quite low, it was felt that only pairs of features should be used. A Fishers linear discriminant function was used to classify each set of images based on the feature values for that set. These classifiers are the optimal linear classifiers if the two classes being considered have multivariate normal distributions with equal covariances. They do not necessarily provide the maximum likelihood classifier.

To determine the 'best' pair of features for each zone or pair of zones, the training results for each possible feature pair combination were computed and ranked based on the total percentage correct for both classes. If two pairs of features had the same total percentage correct, the one with the higher percentage correct for the abnormal class was given a higher ranking. The 'best' pair was chosen from the top ten pairs ranked in this manner. In most cases the pair ranked number one was chosen, however in two instances it was found that there was a large discrepancy between the correct rates for the abnormal and normal samples. In these cases a lower ranking pair was chosen. The best feature pairs for each zone or pair of zones are presented in Table 1. Testing results were obtained for each set of data using the best feature pairs. A one-at-a-time removal procedure was used to obtain the testing results. This involves training on N-1 samples and then submitting the removed sample for classification. This procedure is repeated until each of the N samples has been classified. The testing results are presented in Figures 2, 3, 4 and 5.

Downloaded From: http://proceedings.spiedigitallibrary.org/ on 06/16/2016 Terms of Use: http://spiedigitallibrary.org/ss/TermsOfUse.aspx

As confusion matrices of the following form:

		Computed Class N	Computed Class A	
True Class	N	a	b	% correct for normals
	A	c	d	% correct for abnormals
				total % correct

a = true negatives (correct normals)
b = false positives (normals called abnormals)
c = false negatives (abnormals called normals)
d = true positives (correct abnormals)

Concluding Remarks

Pairs of texture measures have been used in conjunction with four different techniques to classify regions of the lungs of chest x-rays as normal or abnormal. Most of the testing results for the classification of individual zones and bilateral pairs of zones are quite encouraging. Correct rates of 73% to 100% were achieved for all but two of these sets of data. The results for horizontally and vertically adjacent pairs of zones are not as promising, however the poor testing rates could have been caused by over-training. Further study, using much larger sets of data should be done.

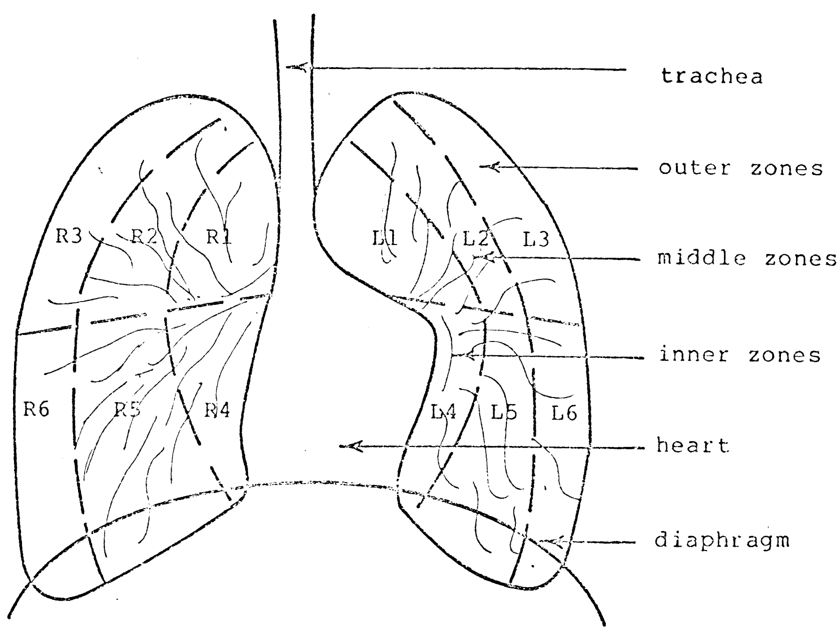

Figure 1 Division of the lungs into twelve zones.

Downloaded From: http://proceedings.spiedigitallibrary.org/ on 06/16/2016 Terms of Use: http://spiedigitallibrary.org/ss/TermsOfUse.aspx

	RIGHT LUNG		LEFT LUNG	
	upper	lower	upper	lower
outer	dist.2, 0°, con dist.1,90°, ent	dist.2, 0°, dmean dist.2,90°, con	dist.2, 0°, con dist.2, 0°, asm	dist.1,90°, asm dist.2,90°, ent
middle	dist.2, 0°, con dist.1,90°, con	dist.1, 0°, deman dist.1,//, con	dist.1,90°, ent dist.1, ⊥, con	dist.1,//, asm dist.2,//, con
inner	dist.1, 0°, asm dist.1,//, dmean	dist.1,90°, ent dist.1,//, con	dist.1, 0°, con dist.1, 0°, ent	dist.2, 0°, ent dist.1,//, con

Table 1(a) Best feature pairs for the individual zones.

	upper	lower
outer	dist.2, 0°, dmean dist.2, 0°, con	first order mean dist.2,90°, con
middle	dist.1,90°, ent dist.2, ⊥, dmean	dist.2,90°, con dist.1,//, ent
inner	dist.1, 0, ent dist.1, ⊥, ent	dist.2, 0°, dmean dist.1,90°, con

Table 1(b) Best feature pairs for the bilateral pairs of zones.

	RIGHT LUNG		LEFT LUNG	
	upper	lower	upper	lower
middle / outer	dist.1, 0°, ent dist.2, ⊥, con	dist.1, 0°, dmean dist.2, 0°, ent	dist.1,90°, asm dist.2, ⊥, con	first order var. dist.1,//, ent
inner / middle	dist.1, 0°, dmean dist.2, 0°, dmean	dist.1,//, dmean dist.2,//, dmean	dist.1, 0°, dmean dist.1, 0°, con	dist.1,90°, dmean dist.2, ⊥, asm

Table 1(c) Best feature pairs for the horizontally adjacent pairs of zones.

	RIGHT LUNG	LEFT LUNG
outer	dist.1, 0°, dmean dist.1,90°, dmean	dist.1, 0°, con dist.2, 0°, ent
middle	dist.1, 0°, con dist.2,//, con	dist.1,//, con dist.1,//, ent
inner	dist.2,90°, asm dist.2, ⊥, con	dist.1, 0°, con dist.1,90°, asm

Table 1(d) Best feature pairs for the vertically adjacent pairs of zones.

Downloaded From: http://proceedings.spiedigitallibrary.org/ on 06/16/2016 Terms of Use: http://spiedigitallibrary.org/ss/TermsOfUse.aspx

	N	A	
N	9	2	81.8%
A	2	9	81.8%
			81.8%

(a) Right lung, upper outer zone.

	N	A	
N	7	3	70%
A	2	8	80%
			75%

(b) Right lung, upper middle zone.

	N	A	
N	9	2	81.8%
A	2	9	81.8%
			81.8%

(c) Right lung, upper inner zone.

	N	A	
N	12	1	92.3%
A	5	8	61.5%
			76.9%

(d) Right lung, lower outer zone.

	N	A	
N	12	0	100%
A	0	12	100%
			100%

(e) Right lung, lower middle zone.

	N	A	
N	15	1	93.7%
A	4	12	75%
			84.4%

(f) Right lung, lower inner zone.

	N	A	
N	8	2	80%
A	2	8	80%
			80%

(g) Left lung, upper outer zone.

	N	A	
N	11	1	91.7%
A	2	10	83.3%
			87.5%

(h) Left lung, upper middle zone.

	N	A	
N	10	2	83.3%
A	2	10	83.3%
			83.3%

(i) Left lung, upper inner zone.

	N	A	
N	7	6	56.8%
A	9	4	30.8%
			42.3%

(j) Left lung, lower outer zone.

	N	A	
N	13	1	92.9%
A	2	12	85.7%
			89.3%

(k) Left lung, lower middle zone.

	N	A	
N	9	2	81.8%
A	2	9	81.8%
			81.8%

(l) Left lung, lower inner zone.

Figure 2 Testing results for the individual zones.

Downloaded From: http://proceedings.spiedigitallibrary.org/ on 06/16/2016 Terms of Use: http://spiedigitallibrary.org/ss/TermsOfUse.aspx

	N	A	
N	10	3	76.9%
A	4	9	69.2%
			73.1%

(a) Upper outer zone.

	N	A	
N	11	3	78.6%
A	4	10	71.4%
			75%

(b) Upper middle zone.

	N	A	
N	12	3	80%
A	0	15	100%
			90%

(c) Upper inner zone.

	N	A	
N	12	5	70.6%
A	3	14	82.3%
			76.5%

(d) Lower outer zone.

	N	A	
N	14	4	77.8%
A	3	15	83.3%
			80.6%

(e) Lower middle zone.

	N	A	
N	8	10	44.4%
A	9	0	50%
			47.2%

(f) Lower inner zone.

Figure 3 Testing results for the bilateral pairs of zones.

Downloaded From: http://proceedings.spiedigitallibrary.org/ on 06/16/2016 Terms of Use: http://spiedigitallibrary.org/ss/TermsOfUse.aspx

	N	A	
N	9	2	81.8%
A	1	10	90.9%
			86.4%

(a) Right lung, upper middle/outer zone.

	N	A	
N	5	6	45.4%
A	5	6	54.5%
			50%

(b) Right lung, upper inner/middle zone.

	N	A	
N	6	7	46.1%
A	9	4	30.8%
			38.5%

(c) Right lung, lower middle/outer zone.

	N	A	
N	9	7	56.2%
A	3	13	81.2%
			68.7%

(d) Right lung, lower inner/middle zone.

	N	A	
N	11	1	91.7%
A	3	9	75%
			83.3%

(e) Left lung, upper middle/outer zone.

	N	A	
N	10	3	76.9%
A	3	10	76.9%
			76.9%

(f) Left lung, upper inner/middle zone.

	N	A	
N	12	3	80%
A	7	8	53.3%
			67.7%

(g) Left lung, lower middle/outer zone.

	N	A	
N	10	4	73.3%
A	5	9	66.7%
			70%

(h) Left lung, lower inner/middle zone.

Fgiure 4 Testing results for the horizontally adjacent pairs of zones.

Downloaded From: http://proceedings.spiedigitallibrary.org/ on 06/16/2016 Terms of Use: http://spiedigitallibrary.org/ss/TermsOfUse.aspx

	N	A	
N	7	7	50%
A	4	10	71.4%
			60.7%

(a) Right lung, outer zone.

	N	A	
N	8	5	61.5%
A	6	7	53.8%
			57.7%

(b) Right lung, middle zone.

	N	A	
N	8	9	47.1%
A	7	10	58.8%
			52.9%

(c) Right lung, inner zone.

	N	A	
N	10	4	71.4%
A	4	10	71.4%
			71.4%

(d) Left lung, outer zone.

	N	A	
N	14	3	82.3%
A	4	13	76.5%
			79.4%

(e) Left lung, middle zone.

	N	A	
N	11	2	84.6%
A	5	8	61.5%
			73.1%

(f) Left lung, inner zone.

Figure 5 Testing results for the vertically adjacent pairs of zones.

References

1. W.W. Ahmed, A.F. Turner and E.L. Hall, "Quantitative diagnosis of early pulmonary edema", Proceedings of the Symposium on Computer Aided Diagnosis of Medical Images, November 1976, pp. 9-13.
2. C.M. Brace, J.H. Kulick and T.W. Challis, "Automatic rib detection in chest radiographs", Proceedings of the International Joint Conference on Artificial Intelligence, 1977.
3. T.W. Challis, C. Skinner, C.M. Berghout and J.H. Kulick, "Automatic analysis of local tissue texture in intercostal spaces of chest roentgenograms", presented at RSNA Conference, November 1976.
4. Y.P. Chien and K.S. Fu, "Recognition of x-ray picture patterns", IEEE Transactions on Systems, Man and Cybernetics, Vol. SMC-4, No. 2, March 1974, pp. 145-156.
5. E.L. Hall, W.O. Crawford and F.E. Roberts, "Computer classification of pneumoconiosis from radiographs of coal workers", IEEE Transactions on Biomedical Engineering, Vol. BME-22, No. 6, November 1975, pp. 518-527.
6. J.R. Jagoe and K.A. Patton, "Measurement of pneumoconiosis by computer", IEEE Transactions on Computers, Vol. C-25, No. 1, January 1976, pp. 95-97.
7. R.P. Kruger, W.B. Thompson and A.F. Turner, "Computer diagnosis of pneumoconiosis", IEEE Transactions on Systems, Man and Cybernetics, Vol. SMC-4, No.1, Jan. 1974, pp. 40-49.
8. J.H. Kulick, T.W. Challis, C. Brace, S. Christodoulakis, I. Merritt and P. Neelands "An image processing laboratory for automated screening of chest x-rays", Proceedings of the Third International Joint Conference on Pattern Recognition, Nov. 1976, pp. 233-237.
9. R.S. Ledley, H.K. Huang and L.S. Rotolo, "A texture analysis method in classification of coal workers pneumoconiosis", Computers in Biology and Medicine, Vol. 5, June 1975, pp. 53-67.
10. A.M. Savol, C.C. Li, T.W. Sze, K. Preston Jr., and D. Sashin, "An algorithm for the detection of small, rounded opacities in chest x-rays with early pneumoconiosis", Proceedings of the Conf. on Pattern Recognition & Image Processing, June 1977, pp. 70-75.
11. H. Stark and D. Lee, "An optical digital approach to the pattern recognition of coal-workers' pneumoconiosis", IEEE Transactions on Systems, Man and Cybernetics, Vol. SMC-6, No. 11, November 1976, pp. 788-793.
12. R.N. Sutton and E.L. Hall, "Texture measures for automatic classification of pulmonary disease", IEEE Trans. on Computers, Vol. C-22, No. 7, July 1972, pp. 667-676.
13. J. Toriwaki, J. Hasegawa and T. Fukumura, "Recognition of vessel shadows for automated measurements and classification system of chest photofluorograms", Proc. of the Symposium on Computer Aided Diagnosis of Medical Images, November 1976, pp. 1-8.
14. J.S. Weska, C.R. Dyer and A. Rosenfeld, "A comparative study of texture measures for terrain classification", IEEE Transactions on Systems, Man and Cybernetics, Vol. SMC-6, No. 4, April 1976, pp. 269-285.

Downloaded From: http://proceedings.spiedigitallibrary.org/ on 06/16/2016 Terms of Use: http://spiedigitallibrary.org/ss/TermsOfUse.aspx